

DMD 1148333

Metabolites of PPI-2458, a Selective, Irreversible Inhibitor of Methionine Aminopeptidase-2. Structure Determination and In Vivo Activity

Christopher C. Arico-Muendel, Bruce Belanger, Dennis Benjamin, Heather S. Blanchette, Teresa M. Caiazzo, Paolo A. Centrella, Jennifer DeLorey, Elisabeth G. Doyle, Ulrike Gradhand, Sarah T. Griffin, Susan Hill, Matthew T. Labenski, Barry A. Morgan, Gary O'Donovan, Kavirayani Prasad, Steven Skinner, Nazbeh Taghizadeh, Charles D. Thompson, James Wakefield, William Westlin, Kerry F. White

Praecis Pharmaceuticals, Inc., 830 Winter Street, Waltham, MA 02451-1420 (C.A.-M., B.B., D.B., H.S.B., T.M.C., P.A.C., J.D., E.G.D., U.G., S.T.G., S.H., M.T.L., B.A.M., G.O., K.P., S.S., N.T., C.D.T., J.W., W.W., K.F.W.)

Running Title Page

Running title: Active metabolites of PPI-2458, a selective MetAP2 inhibitor

Corresponding author information: Christopher C. Arico-Muendel, GlaxoSmithKline, 830 Winter Street, Waltham, MA 02451. Phone: 781-795-4272. Fax: 781-795-4496. Email: christopher.c.arico-muendel@gsk.com

Number of text pages: 49

Number of tables: 7

Number of figures: 5

Number of references: 34

Number of words in Abstract: 249

Number of words in Introduction: 521

Number of words in Discussion: 1335

Abbreviations: AUC, area under curve; BQL, below quantitation limit; C_{max} , maximum plasma concentration; CL/F, initial dose bioavailability adjusted clearance; CNS, central nervous system; CYP3A, Cytochrome P450 3A; DQF-COSY, double quantum filtered correlation spectroscopy; ELISA, enzyme linked immunosorbent assay; ESI⁺, positive electrospray ionization; HPCD, hydroxypropyl-beta-cyclodextrin; HPLC, high pressure liquid chromatography; HRP, horseradish peroxidase; HUVEC, human umbilical vascular endothelial cell; IV, intravenous; KPO₄, potassium phosphate buffer; K_m , Michaelis binding constant; KTZ, ketoconazole; LC-MS, liquid chromatography – mass spectrometry; LLOQ, lower limit of quantitation; MetAP2, methionine aminopeptidase-2; MRM, multiple reaction monitoring; MTT, methylthiazolyldiphenyl-tetrazolium bromide (Thiazolyl Blue Tetrazolium Bromide); PD, pharmacodynamic; PK, pharmacokinetic; PO, by mouth; QOD, every other day; ROESY,

rotating frame Overhauser effect spectroscopy; RT, HPLC retention time; TFA, trifluoroacetic acid; T_{\max} , time of maximum plasma concentration; TOCSY, total correlation spectroscopy; V_{ss}/F , steady-state volume of distribution; WBC, white blood cell; WFI, water for injection.

ABSTRACT

The natural product fumagillin exhibits potent antiproliferative and antiangiogenic properties. The semisynthetic analogue PPI-2458 demonstrates rapid inactivation of its molecular target, methionine aminopeptidase-2 (MetAP2), and good efficacy in several rodent models of cancer and inflammation with oral dosing, despite low apparent oral bioavailability. To probe the basis of *in vivo* efficacy, the metabolism of PPI-2458 was studied in detail. Reaction phenotyping identified cytochrome P450 3A4/5 as the major source of metabolism in man. Six metabolites were isolated from liver microsomes and characterized by mass spectrometry and nuclear resonance spectroscopy, and their structures were confirmed by chemical synthesis. The synthetic metabolites showed correlated inhibition of MetAP2 enzymatic activity and vascular endothelial cell growth. In an *ex vivo* experiment, MetAP2 inhibition in white blood cells, thymus, and lymph nodes in rats following single dosing with PPI-2458 and the isolated metabolites was found to correlate with the *in vitro* activity of the individual species. In a Phase 1 clinical study, PPI-2458 was administered to patients with non-Hodgkin lymphoma. At 15 mg administered orally every other day, MetAP2 in whole blood was 80% inactivated for up to 48 h, although the exposure of parent was only ~10% that of the summed P450 metabolites. Taken together, the data confirm the participation of active metabolites in the *in vivo* efficacy of PPI-2458. The structures define a metabolic pathway for PPI-2458 that is distinct from that of TNP-470. The high level of MetAP2 inhibition achieved *in vivo* supports the value of fumagillin-derived therapeutics for angiogenic diseases.

Introduction

The fungal metabolite fumagillin (Fig. 1A) has been associated with a potent cytostatic activity on endothelial cells that led to demonstrations of an antiangiogenic effect *in vivo*, thereby offering a novel mechanism for treatment of cancer and other diseases dependent on blood vessel formation (Ingber et al, 1990; Folkman, 2007; Ribatti, 2009; Szekanecz et al, 2009; Mauriz et al, 2010; Yin et al, 2012; Gamba-Sanchez, 2012). An early medicinal chemistry campaign seeking to develop fumagillin analogues as therapeutics culminated in the discovery of the analogue TNP-470 (Marui et al, 1992). This compound potently inhibited tumor progression in a number of animal models, and entered the clinic in 1992. Despite encouraging preliminary findings against several cancers (Folkman, 1998; Bernier et al, 2005; Lefkove et al, 2007), further progress of TNP-470 in the clinic was hampered by dose-limiting CNS toxicity, lack of oral bioavailability, and rapid clearance. The chloroacetimide functionality was found to be highly labile, degrading to an unsubstituted carbamate that was processed further by epoxide hydrolase (Placidi et al, 1995).

The molecular target of fumagillin has been identified as the enzyme methionine aminopeptidase-2 (MetAP2), whose cellular role is to cleave the N-terminal methionine residue from newly synthesized polypeptide chains (Sin et al, 1997; Griffith et al, 1997). A crystal structure of the fumagillin-enzyme complex subsequently revealed a covalent binding interaction, wherein the active site His-231 was irreversibly modified by reaction with the fumagillin spiroepoxide (Liu et al, 1998; Fig. 1B). In this complex, the hexenyl chain of fumagillin mimics the Met thioether functionality, whereas the polyolefinic carboxylate extends out of the active site. PPI-2458 differs from fumagillin in that the polyolefinic chain is replaced

by a carbamoyl-linked D-valinamide moiety (Olson et al, 2003; Arico-Muendel et al, 2009). PPI-2458 has demonstrated efficacy in rodent models for non-Hodgkin lymphoma (Cooper et al, 2006), melanoma (Hannig et al, 2006), and arthritis (Bernier et al, 2004; Hannig et al, 2007; Bainbridge et al, 2007; Lazarus et al, 2008; Brahn et al, 2009; Ashraf et al, 2010; Ashraf et al, 2011). In preclinical studies, PPI-2458 was approximately equipotent in several *in vivo* efficacy models by both oral and parenteral routes of administration, despite an apparently modest oral bioavailability (F% = 6, Arico-Muendel et al, 2009). To resolve this issue, we initiated efforts to identify the metabolites of PPI-2458 and to characterize their MetAP-2 inhibitory activity. Here, we report the structures of the six predominant metabolites formed by exposure of PPI-2458 to liver microsomal preparations from multiple species, and characterize their formation by cytochrome P450. All metabolites retained significant, though varying, MetAP2 inhibitory and antiproliferative activities. We also describe the *in vivo* inhibition of MetAP2 in blood and several tissues of rats found by dosing with the individually synthesized metabolites and comparing with PPI-2458, using an *ex vivo* ELISA assay to determine free MetAP2 levels (Bernier et al, 2004). Lastly we report PK and PD results from two cancer patients treated with PPI-2458 as part of a Phase 1 clinical trial. This study revealed highly efficient inhibition of circulating MetAP2 in conjunction with rapid metabolite formation, confirming the importance of active metabolites in the efficacy of PPI-2458.

Materials and Methods

General. Commercially available reagents and solvents were used as purchased without further purification. Midazolam, nifedipine, 1'-hydroxymidazolam, oxidized nifedipine and ketoconazole were from Ultrafine (Manchester, UK). PPI-2458 was prepared from fumagillin (Arico-Muendel et al., 2009). NADPH (Sigma) was prepared as a 10 or 20 mM stock solution in H₂O. Potassium phosphate buffer (KPO₄) was prepared as a 100 mM stock solution and the pH adjusted to 7.4. Microsomes (human, cynomolgus monkey, beagle dog, Sprague-Dawley rat, and CD1 mouse) and S9 liver fractions (male Sprague-Dawley rat) were obtained from In Vitro Technologies (IVT, Baltimore, MD) or XenoTech (Lenexa, KS). Equal volumes of microsomes derived from male and female were combined for each species. Supersomes containing recombinant human CYP3A4 or CYP3A5 plus P450 reductase were purchased, along with the insect expression system control, from BD Gentest (Franklin Lakes, NJ). Internal LC-MS standards for PPI-2458 consisted of either D-Leucine or D-Valine-d8 analogues. All animals were maintained according to the Praecis Pharmaceutical Institutional Animal Care and Use Committee (IACUC) guidelines, in accordance with the Guide for the Care and Use of Laboratory Animals as adopted by the US National Institutes of Health.

LC-MS analysis of in vitro metabolism of PPI-2458 by liver microsomes.

Sample preparation. Three incubations were prepared for each microsome evaluation: (A) time zero control, (B) no-NADPH control, and (C) complete incubation. A stock solution was prepared for each microsome evaluation by combining 891 μ L of 100 mM KPO₄, 25 μ L male/female pooled microsomes, and 4 μ L 5 mM PPI-2458. Stock solution (230 μ L) was then aliquoted into each of three 1.5 mL microfuge tubes. The tubes were pre-incubated for 5 minutes at 37°C. Time zero control samples were then quenched with 500 μ L CH₃CN followed

by the addition of 20 μL of 10 mM NADPH. No-NADPH control samples were treated with 20 μL H_2O while complete incubation samples received 20 μL of 10 mM NADPH, and the samples were then incubated at 37°C for 20 min with constant shaking at 600 rpm, followed by quenching with 500 μL CH_3CN . The samples were then vortexed briefly, centrifuged at 14,000 rpm, and the supernatants were evaporated under nitrogen for 20 min at 45°C. The samples were then taken up in 100 μL H_2O , recentrifuged, and the supernatants were transferred to autosampler vials for LC-MS analysis. An additional control incubation was performed substituting water in place of PPI-2458. Incubations with male Sprague-Dawley rat liver S9 were performed as described above except that the initial stock solution was prepared by combining 816 μL 100 mM KPO_4 , 100 μL male rat liver S9, and 4 μL 5 mM PPI-2458.

LC-MS for full scan analysis of microsome incubations. Chromatograms were acquired on an Applied Biosystems API 4000 triple quadrupole mass spectrometer operating in ESI^+ full scan mode with acquisition from 300 to 800 amu. LC was performed as follows: column, 2.1 x 150 mm Symmetry C18; mobile phases: A = 85:5:10 H_2O : CH_3CN : 25 mM NH_4OAc (aq), B = 90:10 CH_3CN : 25 mM NH_4OAc (aq); flow rate, 200 $\mu\text{L}/\text{min}$; column temperature, 35°C; injection volume, 20 μL ; gradient, 10% B for 5 min, then 10 \rightarrow 50% B in 30 min.

Inhibition of PPI-2458 metabolism by ketoconazole. Co-incubations of PPI-2458 with KTZ were performed using male human liver microsomes. A stock was prepared by combining 3.161 mL 100 mM KPO_4 , 93.75 μL male human microsomes, and 7.5 μL 5 mM PPI-2458, and divided among 12 microfuge tubes as 217.5 μL aliquots. Duplicate tubes were then treated with 12.5 μL of KTZ stock solutions (10 mM in ethanol) diluted to 2% ethanol-water at the following KTZ concentrations: 200 μM , 20 μM , 2 μM , 200 nM, 0 nM (vehicle) and 0 nM (vehicle, no NADPH). All of the tubes were pre-incubated for 5 min at 37°C prior to addition of 20 μL 20

mM NADPH (or 20 μ L water in the case of the no NADPH control). Final KTZ concentrations were 10 μ M, 1 μ M, 100 nM, 10 nM, or 0 nM in a volume of 250 μ L; final concentrations of PPI-2458 were 150 μ M. The samples were then incubated for 20 min at 37°C with shaking at 600 rpm. The incubations were quenched with 500 μ L of CH₃CN followed by 100 μ L of internal standard solution. The samples were vortexed and then centrifuged at 14,000 rpm for 10 min. A 10 μ L aliquot of each supernatant was transferred to an autosampler vial containing 190 μ L H₂O and the samples were analyzed by multiple reaction monitoring by LC-MS. Area ratios of parent to internal standard were averaged between the duplicates.

LC-MS/MS analysis of KTZ inhibition samples. Chromatograms were acquired on an Applied Biosystems API 3000 triple quadrupole mass spectrometer operating in ESI⁺ mode with monitoring at 442.4, 450.4, 458.4, and 474.4 amu for Q1 mass, and 375.2, 383.3, 391.2, and 231.2 amu for Q3 mass for PPI-2458, PPI-2458-d8 (internal standard), +16 metabolite, and +32 metabolite, respectively. LC was performed as follows: column, 2.1 x 30 mm Clipseus C8; mobile phases: A = 85:5:10 H₂O: CH₃CN: 25 mM NH₄OAc (aq), B = 90:10 CH₃CN: 25 mM NH₄OAc (aq); flow rate, 400 μ L/min; column temperature, 35°C; injection volume, 20 μ L; gradient, 20 \rightarrow 90% B in 3.0 min.

NMR analysis of in vitro metabolism of PPI-2458 by liver microsomes.

Large scale sample preparation. A general procedure for microsomal incubations of PPI-2458 on a 5 mg scale was developed as follows. PPI-2458 and mouse liver microsomes were combined in 100 mM KPO₄ buffer (pH 7.4) and pre-incubated at 37°C for 3 minutes with constant orbital shaking at 600 rpm. After the pre-incubation period, NADPH was added to initiate the reaction. Final concentrations after addition of NADPH were 80 μ g/mL PPI-2458, 40 μ L/mL microsomes, and 1.3 mg/mL NADPH. Incubations proceeded at 37°C with continued

shaking for a total of 60 minutes. An additional aliquot of PPI-2458 (~80 $\mu\text{g}/\text{mL}$) was added 15 minutes into the incubation, and an additional aliquot of NADPH (~0.66 mg/mL) was added 20 minutes into the incubation, in an effort to maximize the yield of metabolites. After 60 minutes, the preparations were centrifuged to remove the microsomes, and the aqueous layer was extracted with dichloromethane (3 x 60 mL). The organic extract was concentrated by rotary evaporation and the resulting residue dissolved in ethanol. Individual metabolites were purified from the metabolite mixture obtained from the microsomal incubations using analytical HPLC and fraction collection. Preparative LC was performed as follows: column, 4.6 x 150 mm Waters Symmetry C18 column; mobile phases: A = H_2O , B = CH_3CN ; flow rate, 700 $\mu\text{L}/\text{min}$; column temperature, ambient; gradient, 20% B for 10 min, then 20 \rightarrow 40% B in 30 min. As necessary, fractions were analyzed by LC-MS to confirm identity and purity. Fractions were pooled to obtain individual metabolites at >90% homogeneity, and lyophilized prior to NMR studies to yield 100 – 500 μg of each metabolite.

NMR Spectroscopy. Samples of metabolites purified from microsomal preparations were dissolved in 20% CH_3CN in D_2O and lyophilized to reduce the NMR signal due to residual water. The lyophilisates were then dissolved in 200 μL of CD_3OD (Cambridge Isotope Laboratories, 99.96% atom D) and transferred to CD_3OD susceptibility matched microcell NMR tubes (Shigemi, Inc., Allison Park, PA; part MMS-005V). Chemically synthesized metabolites were dissolved in the CD_3OD (~10 mg in 1 mL) and tested in standard 5 mm NMR tubes. NMR was performed on a Varian Unity Innova 600 MHz spectrometer operated by the Chemistry Department at Brandeis University, and on a Varian MercuryPlus 400 MHz spectrometer at Praecis Pharmaceuticals, Inc. One-dimensional ^1H spectra were recorded at 25°C on the 600 MHz spectrometer, and at ambient temperature on the 400 MHz spectrometer. One-dimensional

^{13}C and gradient enhanced two-dimensional double quantum filtered correlation (DQF-COSY), total correlation (TOCSY), and rotating Overhauser effect spectroscopy (ROESY) were recorded using standard acquisition and processing parameters.

Chemical synthesis of metabolites. To confirm structures as deduced by LCMS and NMR analysis, and to provide materials in sufficient quantities for in vivo testing, the six major metabolites (M1 – M6) were chemically synthesized (Supplemental Data protocol, references, and Figure 1).

Determination of P450 Enzymes Involved in the Metabolism of PPI-2458. The study employed a reaction phenotyping kit from XenoTech (part no. H0500, version 6). The NADPH regenerating system solution was prepared from 15 mg NADP⁺, 195 μL 1 M glucose-6-phosphate in 100 mM phosphate buffer, 60 μL 325 U/mL glucose-6-phosphate dehydrogenase in 100 mM phosphate buffer, 60 μL 1 M MgCl_2 , and 7.5 mL phosphate buffer, pH 7.4. PPI-2458 (2.5 mL of 10 μg / mL aqueous solution) was diluted into 12.0 mL phosphate buffer, and 725 μL was aliquotted into each of 17 silanized Eppendorf tubes. Human liver microsomes (20 mg / mL) from the phenotyping kit were rapidly thawed from frozen 40 μL aliquots stored at -80°C, and 25 μL of each was added to a separate aliquot of PPI-2458 / buffer mixture. Each PPI-2458 / microsome sample was then divided into 4 aliquots of 150 μL each (one T_0 sample plus triplicate reaction runs). Samples were equilibrated at 37°C for 5 minutes, and T_0 samples were then immediately quenched with 500 μL CH_3CN , then treated with NADPH regenerating solution. The other samples were treated with 100 μL NADPH regenerating solution, mixed, and quenched with CH_3CN after 4 min of incubation. Internal standard solution (2 μL of deuterated PPI-2458, 1 mg / mL in ethanol) was then added to each sample. Samples were then each diluted with 250 μL water, vortexed and centrifuged at 14,000 rpm for 10 min, and 80 μL

of supernatant were then further diluted with 120 μL water and analyzed by LC-MS/MS MRM for parent, +16, and +32 metabolites. Chromatograms were acquired on an Applied Biosystems API 4000 triple quadrupole mass spectrometer operating in ESI^+ mode with MRM Q1 and Q3 transition mass (amu) as follows: PPI-2458, 442.4 and 375.2; PPI-2458-d8 (internal standard), 450.4 and 383.3; +16 metabolites, 458.4 and 391.2; +32 metabolites, 474.4 and 231.2. LC was performed as follows: column, 2.1 x 150 mm Symmetry C18; mobile phases: A = 85:5:10 H_2O : CH_3CN : 25 mM NH_4OAc (aq), B = 95:5 CH_3CN : 25 mM NH_4OAc (aq); flow rate, 200 $\mu\text{L}/\text{min}$; column temperature, 35°C; injection volume, 20 μL ; gradient, 10% B for 5 min, then 10 \rightarrow 50% B in 30 min.

Inhibition of P450s in microsomal preparations and kinetics of PPI-2458 by recombinant CYP3A4 and CYP3A5.

Enzyme Assays. Microsomal incubations were carried out in silanized microcentrifuge tubes at 37°C in a Thermomixer (Eppendorf, Hauppauge, NY) with constant mixing at 400 rpm. Microsomes were initially diluted to 5 times (5X) the final concentrations in cold phosphate buffer and kept on ice along with a 5X NADPH-generating solution. Substrate and inhibitor stock solutions were diluted into water, and final incubation mixtures contained 0.45% acetonitrile or less. Aliquots of the 5X NADPH-generating solution were warmed in the mixer for at least 5 minutes prior to use. Microsomes were pre-incubated for 5 or 10 minutes with the test articles by adding 40 μL of the cold 5X microsome suspension to 120 μL of warmed substrate \pm inhibitor solution in the mixer. Incubations were initiated by adding 40 μL of 5X NADPH-generating solution. The final incubation volume was 200 μL and contained 1.0 mM NADP^+ , 5.0 mM glucose-6-phosphate, 1.0 U/mL glucose-6-phosphate dehydrogenase, 3.0 mM magnesium chloride and 50mM phosphate buffer. The reactions were halted by protein

precipitation, transferring 100 μL of the mixtures to 600 μL of ice-cold 80% acetonitrile containing PPI-2458 D-Leu analogue as internal standard. Matrix standards were prepared by stepwise additions of product solutions and each incubation mixture component to cold internal standard solution. Samples and standards were stored at -20°C and then centrifuged at 14,000 rpm for 10 minutes. The supernatants were decanted into fresh silanized microcentrifuge tubes and either diluted 1:20 into 10% CH_3CN or dried under nitrogen in a TurboVap (Zymark, Hopkinton, MA) set to 55°C and reconstituted in 100 μL of 10% CH_3CN for quantitation by LC-MS/MS.

Initial rate conditions and estimates of K_m were established by incubating 1.5-15 μM midazolam, 7.5-50 μM nifedipine or 15-55 μM testosterone for 1-8 min in the presence of 0.1 or 0.2 mg/mL human liver microsomes. Inhibition of 1'-hydroxymidazolam, oxidized nifedipine and 6 β -hydroxytestosterone formation by 0.02-0.5 μM ketoconazole or 25-400 μM PPI-2458, in the presence of 0.05 or 0.2 mg/mL human liver microsomes, was evaluated over a range of 1.5-9 μM midazolam, 20-100 μM nifedipine or 25-150 μM testosterone for 1-4 min. The kinetics of formation for the four major single oxidation metabolites of PPI-2458 by CYP3A4 and CYP3A5 Supersomes were evaluated over a range of 25-800 μM in the presence of 40 nM P450, 80 nM P450 or 40 nM P450 plus 40 nM equivalent insect cell protein control for 3-18 min.

LC/MS/MS Analysis. Samples (5-25 μL injections) were analyzed by LC-MS/MS using an API 3000 (Applied Biosystems, Framingham, MA) triple quadrupole mass spectrometer in ESI^+ ionization mode with MRM Q1 and Q3 transition mass (amu) as follows: midazolam, 326.1 and 291.1; 1'-hydroxymidazolam, 342.2 and 203.2; nifedipine, 347.2 and 254.3; oxidized nifedipine, 345.1 and 284.3; testosterone, 456.3 and 389.2; 6 β -hydroxytestosterone, 305.2 and 269.2; +16 metabolites, 458.4 and 391.4; +32 metabolites, 474.3 and 231.1; PPI-2458, 442.3 and 375.2; PPI-2458-Leu (IS), 456.3 and 389.2. HPLC mobile phases were as follows: A =

85:5:10 H₂O: CH₃CN: 25 mM NH₄OAc (aq), pH 3.5; B = 90:10 CH₃CN: 25 mM NH₄OAc (aq), pH 3.5. Probe substrate metabolites were monitored using a Clipseus C8 column (5 μm; 2.1 x 30 mm; Higgins Analytical, Mountain View, CA), with a linear gradient of 20 → 90% B over 3 min at a flow rate of 0.4 mL/min. PPI-2458 metabolites were monitored using a Symmetry C18 column (3.5 μm; 2.1 x 50 mm; Waters, Milford, MA), with a gradient of 15 → 22%B over 3 min and 22 → 90% B over 3 min at a flow rate of 0.5 mL/min. Column temperatures were maintained at 35°C.

Data Analysis. Kinetic parameters were determined by nonlinear regression analysis of the data using Excel Solver (Version 2002; Microsoft, Redmond, WA). PPI-2458 metabolite production data from recombinant CYP3A4 and CYP3A5 incubations were fit to the Michaelis-Menten model (eq 1). CYP3A substrate inhibition data from human liver microsomes incubations with and without inhibitor were simultaneously fit to the Michaelis-Menten model of competitive inhibition (eq 2), as well as several models of atypical kinetics (Galetin et al., 2003) for single binding site positive cooperative inhibition or negative cooperativity with partial inhibition (eq. 3 and 4), as well as multiple binding site substrate inhibition or heterotropic inhibition (not shown).

$$v = \frac{V_{\max}[S]}{K_m + [S]} \quad (1)$$

$$v = \frac{V_{\max}[S]}{K_m \left(1 + \frac{[I]}{K_i} \right) + [S]} \quad (2)$$

$$v = \frac{V_{\max} \left(\frac{[S]}{K_s} + \frac{\gamma[S][I]}{\delta K_s K_i} \right)}{1 + \frac{[S]}{K_s} + \frac{2[I]}{K_i} + \frac{[I]^2}{\alpha K_i^2} + \frac{[S][I]}{\delta K_s K_i}} \quad (3)$$

$$v = \frac{V_{\max} \left(\frac{[S]}{K_s} + \frac{[S][I]}{\delta K_s K_i} \right)}{1 + \frac{[S]}{K_s} + \frac{[I]}{K_i} + \frac{[S][I]}{\delta K_s K_i}} \quad (4)$$

where α , γ , and δ correspond to interaction factors associated with inhibitor binding affinity, efficiency of product formation, and substrate binding affinity, respectively.

The choice of best fitting model was based on a minimized sum of the squared residuals (SSR), the average SSR from 100 Monte Carlo simulations, visual inspection of the fit and simplicity of the model. A weighting factor of $1/y$ was used in the final inhibition kinetics analysis.

MetAP2 and HUVEC activity. Metabolites were tested against hMetAP2 and HUVEC as described previously (Arico-Muendel et al, 2009). For the HUVEC assay, metabolites were tested at final concentrations ranging from 0.02 pM to 2 μ M.

***In vivo* MetAP2 inhibition by PPI-2458 and metabolites in rodents.**

Compound formulation. PPI-2458 and metabolites were formulated in 11% HPCD in WFI at 0.03, 0.06, and 0.3 mg / mL.

Species. Male Sprague-Dawley rats (200-225 g) were purchased from Charles River Laboratories and housed 2 per cage, with water and chow available *ad libitum*, and allowed to acclimate 5 days prior to the study start.

Dose. Animals administered test articles PO were dosed using 18G feeding needles and 3 cc syringes. Animals administered test article IV were dosed using 25G butterfly infusion sets and 5 cc syringes. Each study group contained 3 animals. PPI-2458 and M1, M2, M3, and M4 were each dosed IV at 0.3 mg / kg, and PO at 0.3 and 3.0 mg / kg.

Sample collection. Blood (approximately 500 μ L) was collected from the jugular vein of each conscious rat ~4 hours following compound administration. Approximately 24 hours following compound administration, animals were anesthetized using Isoflurane inhalant anesthetic and blood was collected via cardiac puncture prior to sacrificing animals with carbon dioxide. Following euthanasia, the lungs, liver, thymus, and pooled lymph nodes (various, not including mesenteric) were collected from each animal.

Sample preparation. Immediately following 4 hour collection, blood was placed into microtainers containing EDTA. Samples were placed briefly on a tilt table, then centrifuged at 6000g for 8 min in an Eppendorf centrifuge (Brinkmann Inc., Westbury NY). Plasma supernatant was pipetted into 1.2 mL silanized Eppendorf tubes (Corning, Corning NY) and stored at -80°C until analysis. Immediately following 24 hour collection, approximately 500 μ L of each sample was placed into microtainers containing EDTA, then processed to plasma as at 4 hours. The remaining blood samples, ~ 5 mL/rat, were placed into 5 mL tubes containing EDTA, then pooled by study group into 50 mL conical tubes and placed on ice until analyzed for MetAP2 content. Organs were immediately snap frozen with liquid nitrogen and stored at -80 °C until analysis.

Plasma sample analysis. Plasma samples were thawed to room temperature to determine drug levels of PPI-2458 and metabolites. For each sample, 200 μ L was transferred to a microcentrifuge tube to which 50 μ L of a 50 ng / mL solution of PPI-2458-d8 was added as an

internal standard. Standard curves were prepared for each analyte in blank plasma over a compound range from 0.1 – 100 ng / mL. Plasma protein was precipitated by adding 500 μ L of acetonitrile and vortexing. The tubes were then centrifuged at 14,000 rpm for 10 min at room temperature. The resulting supernatants were transferred to clean microcentrifuge tubes and dried under nitrogen for 30 min at 80°C. The samples were then reconstituted with water to ~100 μ L, followed by vortexing and centrifugation. The resulting supernatants were transferred to autosampler vials, and 40 μ L were injected onto a Cliepus C8 HPLC column and separated by a 4.5 min gradient elution. LC-MS/MS analysis was achieved with an API 4000 triple quadrupole mass spectrometer using multiple reaction monitoring data acquisition including transitions for PPI-2458 (442 \rightarrow 375), PPI-2458-d8 internal standard (450 \rightarrow 383), and a single transition appropriate to metabolites (458 \rightarrow 391 for M1-M4). Quantitation was performed using Analyst 2.1 software (PE Sciex).

Determination of in vivo MetAP2 inhibition. Whole blood samples were lysed for 30 min at 2 – 8°C (50 mM TrisHCl, pH 7.4; 1% NP-40 (Calbiochem), 0.25% Na deoxycholate, 150 mM NaCl, 1 mM EDTA, 2 mM Na₃VO₄, 1 mM NaF), vortexed, centrifuged 10 min at 13-14 K rpm, decanted, and supernatants frozen and stored at -80°C. Tissue samples (~0.2 g each) were homogenized in disposable tissue grinders (Corning) in ~5 volumes of PBS and complete protease inhibitor. Samples were then treated with 120 mL of 10% NP-40 in PBS, centrifuged, and supernatants frozen and stored at -80°C. Levels of free MetAP2 were quantitated as described previously (Bernier et al, 2004). Briefly, samples were treated with a biotinylated analogue of PPI-2458 to covalently label all non-inhibited MetAP2 in the sample. The complex of MetAP2 with inhibitor-biotin conjugate was then captured on streptavidin plates (Pierce) and detected in ELISA format using an anti-MetAP2 antibody.

PK / PD of PPI-2458 in man

Study design, subjects, and dosing. This was an open label, Phase 1 safety / tolerance study of PPI-2458 in patients with non-Hodgkin's lymphoma. The study was conducted at Dana Farber Cancer Institute, Boston, MA. Written informed consent was obtained from each patient after explanation of the aims, methods, anticipated benefits, and potential hazards of the study. Informed consent was obtained before any study-related procedures were performed. The study was conducted in accordance with generally accepted standards for the protection of subject safety and welfare and in compliance with the informed consent regulations of 21 CFR §50, institutional review board / ethics committee regulations of 21 CFR §56, and the principles of the Declaration of Helsinki and its amendments.

Two patients were enrolled in the initial cohort of the study. Patient 01-01 was a 70-year-old Caucasian female who weighed 61.9 kg; her diagnosis was diffuse large B cell lymphoma. Patient 01-02 was a 66-year-old Caucasian male who weighed 104.5 kg; his diagnosis was follicular lymphoma. The planned dosing schedule was for 15 mg PPI-2458 administered PO (capsules) QOD for 21 days (11 doses total), followed by a 7-day recovery period. Patient 01-01 completed 21 days of dosing and was withdrawn from the study due to disease progression. Due to a pre-clinical neurotoxicity finding, patient 01-02 was withdrawn from the study on Day 5 of dosing, and the study was terminated.

Sample collection and analysis. Samples for pharmacokinetic analyses were collected before the initial dose and at the following sampling times following the first dose: 15 minutes, 30 minutes, 1 hour, and 2, 3, 4, 6, 8, 24, and 48 hours. Pharmacokinetic samples were also scheduled for collection at pre-dose and at 4 hours post dose on Day 15. Processing of pharmacokinetic samples was performed at Charles River Laboratories, Worcester, MA. Specifically, an LC-MS/MS method was developed to quantitate levels of PPI-2458 and the four

+16 metabolites in blood plasma, following precipitation of plasma protein, evaporation, and sample reconstitution. The method was validated for the analysis of PPI-2458 in 200 μL human plasma samples over a concentration range from 0.0200 ng/mL to 10.0 ng/mL in 200 μL sample volumes, and from 5.00 ng/mL to 2500 ng/nL in 100 μL sample volumes. Aliquots of study samples were transferred to 2 mL 96 deep well plates. To these were added 50 μL of PPI-2458-d8 internal standard at 2 ng / mL and 100 ng / mL for low range and high range samples, respectively. Samples were then treated with 50 μL 95:5 H_2O : CH_3CN and briefly vortexed. Samples were then precipitated with 400 μL (high range) or 800 μL (low range) CH_3CN , and centrifuged at 3250 rpm for 10 min. Aliquots of supernatant (400 μL , high range; 800 μL , low range) were then evaporated to dryness under nitrogen at 55°C in a Turbovap concentrator. The dried residues were then reconstituted with 100 μL of 90:10 H_2O : CH_3CN . Quantitation was performed using LC conditions as follows: column, 2.0 x 20 mm Phenomenex Mercury MS Luna C8; mobile phases: A = 85:5:10 H_2O : CH_3CN : 25 mM NH_4OAc (aq, pH 3.5), B = 90:10 CH_3CN : 25 mM NH_4OAc (aq, pH 3.5); flow rate, 700 μL / min; injection volume: 30 μL (low range), 5 μL (high range); gradient, 20% B for 0.5 min, then 20 \rightarrow 60% B in 1.1 min, then 60 \rightarrow 90% B in 0.1 min. Chromatograms were acquired on an Applied Biosystems API-4000 triple quadrupole mass spectrometer operating in ESI^+ mode with MRM Q1 and Q3 transition mass (amu) as follows: PPI-2458, 442.4 and 375.2; PPI-2458-d8 (internal standard), 450.4 and 383.3; +16 metabolite, 458.4 and 391.2; +32 metabolite, 474.4 and 231.2. Chromatograms were integrated using Applied Biosystems Analyst software, and plasma concentrations of the metabolites were determined from peak areas and averaged response factors of the appropriate calibration standards.

Pharmacodynamic analyses were performed on white blood cell lysates obtained pre-first-dose; 4 hour, 24 hour, and 48 hours (prior to second dose); and on Day 15 pre-dose and 4 hours post-dose for patient 01-01. For patient 01-02, the Day 15 samples were not obtained due to withdrawal from the study. Blood samples of 4 mL were collected into 4 mL Sodium Citrate Vacutainer Tubes (Becton-Dickinson 362760) and mixed gently by inversion. They were then centrifuged at room temperature in a swinging bucket rotor for 30 – 45 min at 1700 x g to separate red blood cells. Mononuclear cells and platelets were then resuspended into plasma and decanted. The cell suspension was then diluted to 11 mL with cold PBS, divided into two 5 mL aliquots. Each tube was further diluted with 10 mL cold PBS and centrifuged at 500 x g in a swinging bucket rotor for 10 min at 4 °C. The duplicate cell pellets were then frozen and stored at ≤ -70 °C and shipped to TGA Sciences in Medford, MA for further processing. Free MetAP2 levels were determined by ELISA as described above (Bernier et al, 2004). Total protein content in the lysates was determined using the bicinchoninic acid (BCA) method (Stoscheck, 1990).

Results

Identification of metabolites. PPI-2458 was incubated with microsomes from five species (mouse, rat, dog, monkey, human), and the products were analyzed by LC-MS. Four prominent metabolite peaks were generated by all species evaluated. All four of these metabolites (M1, RT=26.7 min; M2, RT=20.8 min; M3, RT=20.1 min; M4; RT=17.6 min) had molecular ion masses of 441, corresponding to an addition of 16 amu and consistent with the addition of one oxygen atom into the molecular structure of PPI-2458 (Supplemental Figure 2). The intensity of these metabolite peaks correlated with the CYP3A activity of the microsomes as obtained from the supplier (ie, mouse and monkey > human and dog). Likewise, microsomal metabolism of PPI-2458 was efficiently blocked by KTZ, a potent inhibitor of CYP3A, with $IC_{50}[KTZ] \sim 100$ nM. Additional metabolite peaks of lower intensity and earlier retention times were also observed in some of the samples. These peaks had molecular ions corresponding to addition of 32 (M5, M6; incorporation of two oxygen atoms) or 2 amu (incorporation of one oxygen (+16) and demethylation (-14)) relative to PPI-2458. Incubations with rat S9 revealed the formation of a glutathione conjugate of PPI-2458 (RT 20.8 min, $m/z = 732$) in addition to M1 – M4. The formation of this conjugate was independent of NADPH and its mass was consistent with direct addition to the parent compound.

Analysis of product ion spectra of the prominent +16 amu metabolites in comparison with that of PPI-2458 provided little structural information due to the complex fragmentation patterns of these molecules. It was possible to determine that M1, with a retention time of 26.7 min, had undergone modification on the valine moiety of PPI-2458. It was also apparent that the other +16 metabolites were unmodified on valine. The +16 metabolites with retention times of 20.1 and 20.8 min, in particular, had nearly identical fragmentation patterns suggesting that these two metabolites might be stereoisomers. To establish the detailed structures of M1 – M6,

representing the most prominent metabolites, microsomal preparations were generated at a large scale, and samples of each metabolite was isolated in sufficient quantity for NMR (~100 μg in low volume, susceptibility-matched NMR tubes). The structures deduced by NMR were then confirmed by chemical synthesis and are shown in Figure 2. In all cases, NMRs of the synthetic compounds closely matched those of the microsomal isolates (Supplemental Figure 3). ^1H NMR assignments for the metabolites are presented with those of PPI-2458 (Supplemental Table 1).

M1. In agreement with the MS data, the NMR of M1 showed a loss of the βCH D-Val resonance (H19) at 2.04 ppm in PPI-2458. In addition, the αCH and γCH_3 resonances (H20 and Me18) shifted downfield and collapsed to singlets. The data are thus consistent with β -hydroxylation of the PPI-2458 valine moiety. Chemical synthesis of M1 was accomplished by acylation of the N-hydroxysuccinimidyl carbonate ester of fumagillol with H-D- β -hydroxyvaline amide, which was prepared in five steps from methyl (*S*)-(-)-3-(*tert*-butoxycarbonyl)-2,2-dimethyl-4-oxazolidinecarboxylate (Supplemental Figure 1).

M2 and M3. Metabolites M2 and M3 eluted with very similar retention times by LC (Supplemental Figure 2), and their NMR spectra were also found to resemble each other. The distinguishing features of each were the disappearance of the olefinic proton H3 at 5.24 ppm, the appearance of new signals near 3 ppm, and the upfield shift of the prenyl methyl groups (Me1 and Me2) to ~1.3 ppm. These data are consistent with nonstereospecific epoxidation of the side chain double bond, rather than hydroxylation at a single carbon. The NMR spectra of M2 and M3 differ only slightly, with the most noticeable dissimilarities in the region between 1.5 and 3 ppm containing H3, 4, 5, and 6. H3 and H6 could be distinguished from each other by ROE's between H3 and H2, and between H6 and H11.

M2 and M3 could be synthesized simultaneously by treatment of PPI-2458 with dimethyldioxirane (DMDO), generated *in situ* from potassium peroxomonosulfate and acetone, followed by resolution of the diastereomers by preparative HPLC. A tentative stereospecific assignment of M2 and M3 was achieved by oxidation of PPI-2458 with Shi's fructose-based catalyst, 1,2:4,5-di-*O*-isopropylidene- β -D-*erythro*-2,3-hexodiulo-2,6-pyranose (Wang et al, 1997). A single species was produced which coeluted with M2. In analogy with the determinations published by Shi and coworkers, the structures of M2 and M3 were assigned to the *R* and *S* configurations at C3, respectively, as shown in Figure 2.

M4. The NMR spectrum of M4 shows a disappearance of a methyl singlet corresponding to Me2 in the spectrum of PPI-2458, and the appearance of a two-proton singlet at 3.9 ppm. The resonance of H3 also shifts downfield by over 0.2 ppm. These data suggest hydroxylation of C2 to form M4.

Chemical synthesis of M4 was accomplished by oxidation of PPI-2458 with SeO₂, which is known to yield the *trans*-allylic alcohol when applied to prenyl groups (Bhalerao and Rapoport, 1971). The NMR of the synthetic product lacked two small signals seen in the authentic metabolite at 1.9 and 4.1 ppm, although the major signals were in good alignment (Supplemental Figure 3). This suggests that M4 consists predominantly of the *trans* allylic alcohol, with a minor component of the *cis* alcohol, in an approximate ratio of 5 to 1 (Fig. 2).

M5 and M6. MS studies indicated that M5 and M6 were doubly oxidized (+32) with one oxygen on the D-Val. NMR spectra of the compounds were found to combine features of the spectra of M1 and M2 for M5, and M1 and M3 for M6. The structures of M5 and M6 were thus assigned as diastereomeric hydroxyvaline triepoxides, which were confirmed synthetically by DMDO oxidation of M1.

Interaction of metabolites with Cytochrome P450.

Determination of P450 enzymes. A reaction phenotyping kit consisting of human liver microsomes from 16 individuals and one pooled microsomal mixture was used to identify which CYP enzymes were primarily responsible for the metabolism of PPI-2458. Initial rate conditions were determined by monitoring the disappearance of 1 $\mu\text{g} / \text{mL}$ PPI-2458 incubated with varying concentrations of pooled human liver microsomes (0.05, 0.1, 0.2, and 0.4 mg / mL). PPI-2458 (1 $\mu\text{g} / \text{mL}$) was then incubated with 0.40 mg / mL microsomes from individuals for 4 min, and the formation of primary metabolites M1 – M4 was tracked by LC-MS/MS. Table 1 shows the Pearson product moment correlation coefficients (R) produced by comparison of the normalized metabolite peak areas to the CYP3A4 and CYP3A5 enzyme activity levels reported for each test microsome. All oxidation metabolites were strongly correlated ($R > 0.75$) with CYP3A4/5 activity, and weakly correlated ($R > 0.45$) with CYP2C19 activity.

Kinetics of metabolite formation. PPI-2458 was incubated with recombinant CYP3A4 and CYP3A5 to compare the metabolite production kinetics of M1 – M4. In each case, linear formation rates were fit to the Michaelis-Menten model, yielding kinetic parameters for recombinant CYP3A4 and CYP3A5 that are shown in Table 2. K_m values for the four oxidations were very similar, differing by less than 2-fold and averaging 19 μM for both enzymes. The intrinsic clearance (V_{max}/K_m) was more variable, ranging from a 3-fold higher CYP3A4 rate for M4 to a 5-fold higher CYP3A5 rate for M1. The average rates across all the metabolites, however, were comparable: 0.12 $\mu\text{L}/\text{min}/\text{pmol}$ CYP3A4 and 0.094 $\mu\text{L}/\text{min}/\text{pmol}$ CYP3A5.

PPI-2458 inhibition of CYP activity. Concentrations of PPI-2458 up to 40 μM failed to inhibit CYP3A4 mediated oxidation of dibenzofluorescence, whereas KTZ inhibited this reaction with $\text{IC}_{50} = 9.8 \text{ nM}$ (data not shown). To explore the potential for inhibition of other CYP3A

substrates, PPI-2458 was incubated with midazolam, nifedipine, or testosterone in pooled human liver microsomes and compared to inhibition by KTZ. Initial rate conditions, linear with respect to time and microsomal protein concentration, were established and then inhibition was assessed in the presence of 25 – 400 μM PPI-2458 or 0.02 – 0.5 μM ketoconazole. Lineweaver-Burk and Dixon analysis indicated that inhibition by PPI-2458 was consistent with a competitive mechanism. Data was fit to the Michaelis-Menten model of competitive inhibition, as well as to several models of atypical kinetics. The resulting kinetic parameters are shown in Table 3. The Michaelis-Menten model was the best fit for all but KTZ inhibition of nifedipine oxidation, which displayed negative cooperativity. KTZ inhibited the CYP3A mediated formation of 1'-hydroxymidazolam, oxidized nifedipine, and 6 β -hydroxytestosterone with K_i values of 0.007, 0.011, and 0.049 μM respectively. The corresponding K_i values exhibited by PPI-2458 were 58, 403, and 287 μM .

In vitro inhibition of MetAP2 activity and HUVEC proliferation.

Determination of hMetAP2 inhibition. We have reported an assay that is suitable for analysis of slow, tight binding fumagillin-based MetAP-2 inhibitors (Arico-Muendel et al, 2009). Thus, this assay records the fraction of active enzyme remaining during 8-hour incubation with inhibitor. Activities of M1 – M6 in this assay are shown in Table 4. PPI-2458 inhibited MetAP2 to approximately 12% of enzyme-only control in 1 h, and to 3% at 8 h. Of the six metabolites, M1 demonstrated a similar level of activity. M2 and M4 showed slower initial activity but reached ~90% inhibition at the end of the experiment, whereas M3 was only ~40% inhibited at this time. The potencies of M5 and M6 roughly tracked those of M2 and M3, respectively. A non-metabolite analogue of M4, PPI-4338, was nearly inactive.

Inhibition of HUVEC proliferation. HUVEC cultures were incubated with purified metabolites for three days, and the percent cell growth was determined with MTT relative to vehicle control. A representative HUVEC assay is shown in Figure 3, and all the assay data are summarized in Table 4. Under these conditions, M1 exhibited the highest potency, close to that of PPI-2458 ($EC_{50} = 0.3$ nM vs 0.1 nM). The activity of M2 was reduced ~10 fold, to 1.3 nM, whereas the remaining metabolites inhibited near 10 nM.

Metabolite PD and PK studies.

MetAP2 inhibition following single dose administration of PPI-2458 in rats. An ELISA based assay was employed to determine free MetAP2 levels in rat blood and tissue samples following treatment with PPI-2458 and its synthesized metabolites. Briefly, cells were lysed and treated with a PPI-2458 – biotin conjugate, which enabled capture of free MetAP2 onto immobilized streptavidin and detection / quantitation by an anti-MetAP / HRP dual antibody system (Bernier et al, 2004). Compounds were administered as single doses, either IV or PO, at 0.3 and 3.0 mg / kg. To follow up earlier research suggesting the utility of PPI-2458 for treatment of non-Hodgkin's lymphoma (Cooper et al, 2006), samples were collected from blood, lungs, lymph nodes and thymus 24 h after administration. Free MetAP2 levels, as a percentage of vehicle, are shown in Figure 4. Following IV administration, similar profiles for average free MetAP2 levels in different compartments were observed across all the compounds tested; however, individual measurements except for blood were also highly variable. In contrast, PPI-2458 and the metabolites exhibited more differentiated activity following oral administration. PPI-2458 and M1 showed similar levels of inactivation, followed by somewhat less effective M2, M3, and M4. Thus, significant inhibition by a 0.3 mg/kg dose PO was only observed for PPI-2458 and M1, whereas all compounds were effective at 3 mg/kg. Effectiveness as a function of compartment followed the order blood > liver > lungs > lymph nodes > thymus.

Plasma samples were also obtained for all studies at 4 h and 24 h post dose to assess exposure. For the IV arm, levels of parent and metabolites were below the level of quantitation for all compounds at both time points, and only trace quantities (≤ 0.3 ng/mL) could be detected at the lower oral dose (data not shown). For animals dosed at 3.0 mg / kg PO, quantifiable levels of each analyte could be observed at 4 h for the 3 mg/kg dose, but only for M1 at 24h (Table 5). M2, M3, and M4 could also be detected following a 3 mg / kg PO dose of PPI-2458.

PK / PD studies in man. As part of a Phase 1 dose escalation study, PPI-2458 was administered to two patients with non-Hodgkin's lymphoma. Oral doses of PPI-2458 at 15 mg/kg were given every other day, and plasma samples for PK / PD analysis were collected at 15 min, 30 min, and 1, 2, 3, 4, 6, 8, 24, and 48 h following the first dose, as well as pre- and 4h post-dose on day 15 (one patient). For both subjects, uninhibited (free) MetAP2 levels in white blood cell samples was below the quantitation limit 4h post dose (Table 6), indicating rapid target engagement and inactivation after oral dosing. As a percentage of predose free MetAP2 level, this corresponded to <1.5% and <6.0% for patients 01 and 02, respectively, due to the four-fold difference in predose free MetAP2 (Table 6). For both subjects, inhibition remained high (1.6% and <6.0 % free MetAP2, respectively) for 24h, and showed partial recovery after 48 h (6.6% and 17.1% free MetAP2, respectively).

Levels of PPI-2458 and M1 – M6 were measured to determine pharmacokinetic parameters (Table 7). The exposure profiles for both patients are shown in Figure 5. PPI-2458 accounted for approximately 10% of the total measured exposure, with maximum plasma concentrations of 77.7 and 32.3 ng / mL attained within an hour of initial administration for both subjects. Elimination of PPI-2458 was monophasic, with $t_{1/2} = 2.1$ and 1.1 h. Of the species monitored in the study, the metabolites accounted collectively for nearly 90% of the exposure, with the greatest contribution by M2 (~30%), followed by M3 (~20%). On the other

hand, the exposure due to M1 is almost negligible. Average T_{\max} values within an hour were also observed for M1 – M4, suggesting rapid formation of these species, whereas those for M5 and M6 were slightly longer. An apparent elimination phase followed from the time of the peak metabolite concentrations. Metabolites M2, M3, and M4 had apparent elimination half-lives of approximately 1 hour, whereas M5 and M6 tended to have longer half-lives (closer to 2 hours) during this phase.

For most of the metabolites, a second elimination phase, where metabolite concentrations initially increased and then either stabilized or diminished at a slower apparent elimination rate, was seen after 4 hours post-dose. The slight increases or maintenance of metabolite concentrations occurred from 6 hours to 24 hours post-dose for subject 01 and from 4 hours to 8 hours post dose for subject 02. During this second phase, concentrations of M5 and M6 rose to levels similar in magnitude to those of M2 and M3. M4 showed a trend similar to that of M5 and M6 with lower nominal concentration levels.

Discussion

This study of the metabolism of PPI-2458 was driven by observations of efficacy in animal models for cancer (Cooper et al, 2006; Hannig et al, 2006) and rheumatoid arthritis (Hannig et al, 2007; Lazarus et al, 2008) following oral dosing, despite apparent low oral bioavailability of the parent compound. As a first step towards characterization of PPI-2458 metabolism *in vivo*, we studied the effects of treatment with liver microsomal preparations. Six major species were identified, corresponding to four single and two double oxidation products, as well additional minor species and a glutathione adduct formed in rat S9 preparations. Identification of CYP3A4/5 as playing a key role in the formation of M1 – M6 was suggested by the effectiveness of KTZ in suppressing metabolism, and demonstrated explicitly by phenotyping experiments that showed a clear correlation between the activity of these CYP isoforms and metabolite formation. In addition, measurement of kinetic parameters using recombinant CYP3A4 and CYP3A5 indicated similar intrinsic clearance rates (V_{\max} / K_m) for both enzymes. The proportions of the metabolites formed in microsomes generally parallel the kinetics observed from recombinant CYP3A4/5, where the intrinsic clearance of M1 lags that of M2 – M4. Relative to KTZ, PPI-2458 was found to minimally block CYP metabolism of three representative drugs, with K_i 's in the high micromolar range.

Through a large scale preparation, sufficient quantities of M1 – M6 were isolated and purified to enable 2D NMR studies. As a result, detailed structures for each metabolite could be proposed, which were confirmed by independent chemical synthesis. The structures for M1 – M6 are consistent with CYP mediated oxidation reactions involving attack at specific sites on hydrophobic groups at the periphery of the molecule. Of the few examples of published fumagillin metabolites, it is noteworthy that oxidation of fumagillin with *m*-chloroperbenzoic acid yields a mixture of diastereomeric triepoxides corresponding to M2 and M3 in PPI-2458

(Halász et al, 2000). The same study reported these species as minor impurities in commercial fumagillin resulting from degradation over time. Metabolism of fumagillin derivatives has been studied in the case of TNP-470 (Placidi et al, 1995) and CKD-732 (Myung et al, 2002). *In vivo*, TNP-470 is rapidly degraded to an unsubstituted carbamate by esterases, which in turn is processed by microsomal epoxide hydrolase into an inactive bicyclic structure. For CKD-732, the polyolefinic side chain of this molecule is replaced a cinnamyl ester functionalized with a 4-dimethylaminoethoxy group, whereas the core and the isobutenyl containing C4 substituent are preserved. Microsomal metabolism of CKD-732 yielded a single predominant species, identified as the N-oxide of the dimethylamino moiety, and 13 other species of much lesser abundance that were characterized by LC-MS. Several of these were assigned to oxidations of one of the C4 terminal methyl groups. However, double bond epoxidation as was observed with M2 and M3 in the case of PPI-2458 would also be consistent with the limited MS fragmentation data. An additional modification proposed in several of the metabolites involved opening of the parent epoxide groups by addition of water to form a fused bicyclic structure as in the case of TNP-470. Although we did not observe significant formation of such water adducts in this study, we did find them as significant products of PPI-2458 degradation in acidic conditions (Arico-Muendel et al, unpublished).

Testing the isolated compounds M1 – M6 in hMetAP2 and HUVEC assays demonstrated that the inhibitory activity of PPI-2458 was preserved in all the major metabolites. The good correlation of the biochemical and cellular assays establishes a link between compound-mediated enzyme inhibition and antiproliferative activity in a cell type relevant to angiogenesis. The resulting structure – activity relationships may be considered in light of the published X-ray structure of MetAP2 with fumagillin (Liu et al, 1998). The C4 side chain was found to be deeply buried, mimicking the position of the methionyl substrate side chain, whereas the C6

chain extended towards solvent with relatively little constraint. Accordingly, we and others found that the C6 substituent could be replaced with a variety of groups, with the primary limitation being avoidance of steric clash with two leucine “gatekeeper” residues in the active site (Arico-Muendel et al, 2009; Marui et al, 1992; Lee et al, 2007). Thus, the nearly unaltered activity of M1, whose modification occurs on the C6 group, is not surprising. Alterations to the C4 chain, as occur in M2 – M6, are expected to have more drastic effects; the slightly more constricted pocket in MetAP1, for example, has been cited as a grounds for the selectivity of fumagillin for MetAP2 over MetAP1 (Liu et al, 1998, Addlagatta and Matthews, 2006). Nonetheless, despite clearly diminished activity, all of these retain significant capacity to inhibit MetAP2 (Table 5). M2 and M3, formed by CYP in roughly equal proportions, differ somewhat in their activity as a result of disrupting the planarity of the side chain, with the *R*-configuration apparently better tolerated than the *S*. In M4, hydroxylation to form a *trans* allylic alcohol appears to be accommodated well in the active site. M4 shows reduced HUVEC activity, however, possibly due to reduced cellular permeability. Comparison with the designed compound PPI-4338 also highlights the subtlety of interactions in this pocket. Despite close homology to M2, M3, and M4, PPI-4338 exhibits only minimal inhibition of MetAP2.

The covalent nature of MetAP2 binding by PPI-2458 means that target – inhibitor complexes should be exceptionally stable, facilitating studies of MetAP2 inhibition *in vivo*. Following the guidance of work identifying MetAP2 as the target of fumagillin (Sin et al, 1997; Griffith et al, 1997), we designed a biotinylated derivative of PPI-2458 as a pull-down reagent (Bernier et al, 2004). This conjugate enabled accurate quantitation of free MetAP2 levels from blood or tissue lysates following *in vivo* dosing. Here, we presented results showing high levels of MetAP2 inhibition by both PPI-2458 and its primary metabolites. Oral administration showed a dose dependant response, with the highest level of inactivation observed in whole

blood, liver, and lung for PPI-2458 and M1 at 3.0 mg/kg. Interestingly, under these conditions the compounds roughly segregate according to their enzymatic and antiproliferative activity, with the C4 hydroxylated metabolites significantly attenuated relative to M1 and parent compound. On the other hand, whereas some structural differentiation is still apparent at 0.3 mg / kg PO, the compounds are roughly equivalent, and significantly less effective, at the same dose administered IV. These results may be interpreted in light of the exposure data, which shows clearance of all species within 4 h following IV dosing, but significant levels of PPI-2458 and metabolites at 4 h in the PO arm. Consistent with the notion of PPI-2458 as a slow binding inhibitor, the similar levels of inhibition in the IV experiment may reflect brief exposure to high levels of compound that mask structure-based discriminating effects, which only become apparent under extended exposure to low concentrations.

As part of a proof-of-concept experiment in man, two patients with NHL received PPI-2458 orally at 15 mg QOD. At this dose, PPI-2458 was highly effective at inhibiting MetAP2 in blood, with <20% free enzyme measured at 48h after dosing. Analysis of plasma samples indicated that most of the exposure was due to metabolites, predominantly M2 and M3. The exposure profiles indicate that PPI-2458 is rapidly metabolized favoring M2 and M3 initially. That M1 levels are nearly negligible, whereas the secondary metabolites M5 and M6 appear rapidly, suggests that D-Val hydroxylation is inefficient relative to epoxidation, and that M5 and M6 form primarily via M2 and M3. Since M2 and M3 are somewhat less effective inhibitors of MetAP2, development of second-generation compounds could focus on suppressing this metabolic pathway. Overall, the results accord with the trend observed in primate studies (not shown) that indicate an increasing level of exposure due to metabolites in higher species.

In conclusion, this work has identified the CYP-generated metabolites of PPI-2458 and determined their activity *in vitro*. The metabolites are shown to contribute significantly to

pharmacologically active compound exposure *in vivo*. In man, initial results of a Phase 1 study in patients demonstrate effective inhibition of MetAP2 administered orally.

Acknowledgements

We thank Sara Kunz and Susan Pochapsky of the Department of Chemistry at Brandeis University for assistance with NMR spectroscopy, and Elise Martin at Charles River Laboratories for assistance with PK study data in man.

Authorship Contributions

Participated in research design: Arico-Muendel, Benjamin, Blanchette, Morgan, Thompson, Wakefield, Westlin

Conducted experiments: Arico-Muendel, Blanchette, Caiazzo, DeLorey, Doyle, Gradhand, Griffin, Hill, Labenski, O'Donovan, Prasad, Skinner, Taghizadeh, Thompson, Wakefield, White

Contributed new reagents or analytic tools: Centrella, Labenski

Performed data analysis: Arico-Muendel, Belanger, Benjamin, Blanchette, Caiazzo, DeLorey, Labenski, O'Donovan, Prasad, Skinner, Thompson, Wakefield, White

Wrote or contributed to writing of manuscript: Arico-Muendel, Caiazzo, Gradhand, Wakefield, Westlin

References

- Arico-Muendel CC, Benjamin DR, Caiazzo TM, Centrella PA, Contonio BD, Cook CM, Doyle EG, Hannig G, Labenski MT, Searle LL, Lind K, Morgan BA, Olson G, Paradise CL, Self C, Skinner SR, Sluboski B, Svendsen JL, Thompson CD, Westlin W, and White KF (2009) Carbamate analogues of fumagillin as potent, targeted inhibitors of methionine aminopeptidase-2. *J Med Chem* **52**: 8047-8056.
- Addlagatta A and Matthews BW (2006) Structure of the angiogenesis inhibitor ovalicin bound to its noncognate target, human Type 1 methionine aminopeptidase. *Protein Sci* **15**: 1842-1848.
- Ashraf S, Mapp PI, and Walsh DA (2010) Angiogenesis and the persistence of inflammation in a rat model of proliferative synovitis. *Arthritis Rheum* **62**: 1890-1898.
- Ashraf S, Mapp PI, and Walsh DA (2011) Contributions of angiogenesis to inflammation, joint damage, and pain in a rat model of osteoarthritis. *Arthritis Rheum* **63**: 2700-2710.
- Bainbridge J, Madden L, Essex D, Binks M, Malhotra R, and Paleolog EM (2007) Methionine aminopeptidase-2 blockade reduces chronic collagen-induced arthritis: potential role for angiogenesis inhibition. *Arthritis Res Ther* **9**: R127.
- Bernier SG, Lazarus DD, Clark E, Doyle B, Labenski MT, Thompson CD, Westlin WF, and Hannig G (2004) A methionine aminopeptidase-2 inhibitor, PPI-2458, for the treatment of rheumatoid arthritis. *PNAS* **101**: 10768-10773.
- Bernier S, Westlin WF, and Hannig G (2005) Fumagillin class inhibitors of methionine aminopeptidase-2. *Drugs of the Future* **30**: 497-508.

- Bhalerao UT and Rapoport H (1971) Stereochemistry of allylic oxidation with selenium dioxide. Stereospecific oxidation of gem-dimethyl olefins. *J Am Chem Soc* **93**: 4835-4840.
- Brahn E, Schoettler N, Lee S, and Banquerigo ML (2009) Involution of collagen-induced arthritis with an angiogenesis inhibitor, PPI-2458. *J Pharm Exp Ther* **329**: 615-624.
- Cooper AC, Karp RM, Clark EJ, Taghizadeh NR, Hoyt JG, Labenski MT, Murray MJ, Hannig G, Westlin WF, and Thompson CD (2006) A novel methionine aminopeptidase-2 inhibitor, PPI-2458, inhibits non-Hodgkin's lymphoma cell proliferation in vitro and in vivo. *Clin Cancer Res* **12**: 2583-2590.
- Folkman J (1998) Tumor angiogenesis, in *Accomplishments in Cancer Research 1997* (Wells SA, Sharp PA, eds) pp 32-44, Lippincott Williams & Wilkins, Philadelphia.
- Folkman J (2007) Angiogenesis: an organizing principle for drug discovery? *Nature Rev Drug Disc* **6**: 273-286.
- Gamba-Sanchez D (2012) Fumagillin and structurally related molecules as source of new drugs. *Mini-reviews in Organic Chemistry* **9**: 126-142.
- Galetin A, Clarke SE, and Houston JB (2003) Multisite kinetic analysis of interactions between prototypical CYP3A4 subgroup substrates: midazolam, testosterone, and nifedipine. *Drug Metab Dispos* **31**: 1108-1116.
- Griffith EC, Su Z, Turk BE, Chen S, Chang Y-H, Wu Z, Biemann K, and Liu JO (1997) Methionine aminopeptidase (type 2) is the common target for angiogenesis inhibitors AGM-1470 and ovalicin. *Chemistry and Biology* **4**: 461-471.
- Halász J, Podányi B, Vasvári-Debreczy L, Szabó A, Hajdú F, Böcskei Z, Hegedűs-Vajda J, Györbíró A, and Hermeicz I (2000) Structure elucidation of fumagillin-related natural products. *Tetrahedron* **56**: 10081-10085.

Hannig G, Lazarus DD, Bernier SG, Karp RM, Lorusso J, Qiu D, Labenski MT, Wakefield JD, Thompson CD, and Westlin WF (2006) Inhibition of melanoma tumor growth by a pharmacological inhibitor of MetAP2, PPI-2458. *Int J Oncol* **28**: 955-963.

Hannig G, Bernier SG, Hoyt JG, Doyle B, Clark E, Karp RM, Lorusso J, and Westlin WF (2007) Suppression of inflammation and structural damage in experimental arthritis through molecular targeted therapy with PPI-2458. *Arthritis Rheum* **56**: 850-860.

Ingber D, Fujita T, Kishimoto S, Sudo K, Kanamaru T, Brem H, and Folkman J (1990) Synthetic analogues of fumagillin that inhibit angiogenesis and suppress tumour growth. *Nature* **348**: 555-557.

Lazarus DD, Doyle EG, Bernier SG, Rogers AB, Labenski MT, Wakefield JD, Karp RM, Clark EJ, Lorusso J, Hoyt JG, Thompson CD, Hannig G, and Westlin WF (2008) An inhibitor of methionine aminopeptidase-2, PPI-2458, ameliorates the pathophysiological disease processes of rheumatoid arthritis. *Inflamm Res* **57**: 18-27.

Lee HW, Cho CS, Kang SK, Yoo YS, Shin JS, Ahn SK (2007) Design, synthesis, and antiangiogenic effects of a series of potent novel fumagillin analogues. *Chem Pharm Bull* **55**: 1024-1029.

Lefkove B, Govindarajan B, Arbiser J (2007) Fumagillin: an anti-infective as a parent molecule for novel angiogenesis inhibitors. *Expert Rev Anti Infect Ther* **5**: 573-579.

Liu S, Widom J, Kemp CW, Crews CM, and Clardy J (1998) Structure of human methionine aminopeptidase-2 complexed with fumagillin. *Science* **282**: 1324-1327.

Mauriz JL, Martín-Renedo J, García-Palomo A, Tuñón MJ, and González-Gallego J (2010) Methionine aminopeptidases as potential targets for treatment of gastrointestinal cancers and other tumors. *Current Drug Targets* **11**: 1439-1457.

- Marui S, Itoh F, Kozai Y, Sudo K, and Kishimoto S (1992) Chemical modification of fumagillin. I. 6-*O*-acyl, 6-*O*-sulfonyl, 6-*O*-alkyl, and 6-*O*-(*N*-substituted-carbamoyl)fumagillols. *Chem Pharm Bull* **40**: 96-101.
- Myung S-W, Kim H-Y, Min H-K, Kim D-H, Kim M, Cho H-W, Lee HS, Kim J-K, and Hong CI (2002) The identification of in vitro metabolites of CKD-732 by liquid chromatography / tandem mass spectrometry. *Rapid Commun Mass Spectrom* **16**: 2048-2053.
- Olson GL, Self C, Lee L, Cook CM, and Birktoft JJ (2003) US Patent 6,548,477.
- Placidi L, Cretton-Scott E, de Sousa G, Rahmani R, Placidi M, and Sommadossi J-P (1995) Disposition and metabolism of the angiogenic modulator *O*-(chloroacetyl-carbamoyl) fumagillol (TNP-470; AGM-1470) in human hepatocytes and tissue microsomes. *Cancer Res* **55**: 3036-3042.
- Ribatti D (2009) The discovery of antiangiogenic molecules: a historical review. *Curr Pharm Design* **15**: 345-352.
- Sin N, Meng L, Wang MQW, Wen JJ, Bornmann WG, and Crews CM (1997) The anti-angiogenic agent fumagillin covalently binds and inhibits the methionine aminopeptidase, MetAP-2. *Proc. Natl. Acad. Sci USA* **94**: 6099-6103.
- Stoscheck CM (1990) Quantitation of Protein. *Methods in Enzymology* **182**: 50-68.
- Szekanecz Z, Besenyei T, Paragh G, and Koch AE (2009) Angiogenesis in rheumatoid arthritis. *Autoimmunity* **42**: 563-573.
- Wang Z-X, Tu Y, Frohn M, Zhang J-R, and Shi Y (1997) An efficient catalytic asymmetric epoxidation method. *J Am Chem Soc* **119**: 11224-11235.
- Yin S-Q, Wang J-J, Zhang C-M, and Liu Z-P (2012) The development of MetAP-2 inhibitors in cancer treatment. *Current Medicinal Chemistry* **19**: 1021-1035.

Footnotes

Presented in part at the 8th Meeting of the International Society for the Study of Xenobiotics, 2004.

Send reprint requests to Christopher C. Arico-Muendel, GlaxoSmithKline, GlaxoSmithKline, 830 Winter Street, Waltham, MA 02451-1420. Email: christopher.c.arico-muendel@gsk.com

Current Affiliations:

Christopher C. Arico-Muendel, Gary O'Donovan, Steven Skinner: GlaxoSmithKline, 830 Winter Street, Waltham, MA 02451-1420

Bruce Belanger: Merrimack Pharmaceuticals, 1 Kendall Square # B7201 Cambridge, MA 02141

Dennis Benjamin: Seattle Genetics, Inc., 21823 – 30th Drive SE, Bothell, WA 98021

Heather Blanchette: Cubist Pharmaceuticals, 65 Hayden Avenue, Lexington, MA 02421

Teresa M. Caiazzo: Pfizer Inc., One Burtt Road, Andover, MA 01810

Paolo A. Centrella: X-Chem, Inc., 100 Beaver Street, Waltham, MA 02453

Jennifer DeLorey: 175 Oakdale St Attleboro MA 02703

Elisabeth G. Doyle: Vertex Pharmaceuticals, 130 Waverly Street, Cambridge, MA 02139

Sarah T. Griffin: Chemical Research and Development, Pfizer, Eastern Point Road, Groton, CT 06340

Susan Hill: Merck, 33 Avenue Louis Pasteur, Boston MA 02115

Matthew T. Labenski, William Westlin: Celgene Avilomics Research, 45 Wiggins Avenue, Bedford, MA 01730

Barry A. Morgan: 237 Prospect St., Franklin, MA 02038

Kavirayani Prasad: Department of Organic Chemistry, Indian Institute of Science, Bangalore-560 012, India

Nazbeh Taghizadeh: Brigham and Women's Hospital, 272 Centre Street, Newton, MA 02458

Charles D. Thompson: Merck & Company Incorporated, West Point, PA 19486

James Wakefield: Ironwood Pharmaceuticals, 320 Bent Street, Cambridge, MA 02141

Kerry F. White: Infinity Pharmaceuticals, 780 Memorial Drive, Cambridge, MA 02139

Figure Legends

Fig. 1. (A) Structures of fumagillin and PPI-2458, (B) mechanism of covalent MetAP2 inhibition by fumagillin derivatives.

Fig. 2. Structures of the six major CYP metabolites derived from PPI-2458.

Fig. 3. Inhibition of HUVEC proliferation for M1 – M4.

Fig. 4. Free MetAP2 levels (as percent of vehicle control) in whole blood, liver, lung, thymus, and lymph nodes of male SD rats 24 hours after a single dose of PPI-2458, M1, M2, M3, or M4 administered IV, 0.3 mg/kg (top); PO, 0.3 mg/kg (middle); PO, 3.0 mg/kg (bottom).

Fig. 5. Day 1 pharmacokinetic profile of PPI-2458 and its metabolites following 15 mg PO dose of PPI-2458 in patient 01-01 (top) and patient 01-02 (bottom). Points below the limit of quantitation (BLQ) are arbitrarily set to a concentration of 0.05 ng / mL.

Tables

Table 1. Correlation R-values for metabolite production relative to CYP enzyme activity levels: 1 µg / mL PPI-2458, 0.4 mg / mL human liver microsomes from 16 individuals + 1 pooled microsomal mixture, 4 min triplicate incubations at 37°C. LC-MS/MS reconstructed ion chromatogram peak areas are normalized to PPI-2458-d8 used as internal standard. Enzyme activities were provided by manufacturer.

<u>Metabolite</u>	<u>CYP5</u>				<u>CYP450</u>						
	<u>OR</u>	<u>1A2</u>	<u>2A6</u>	<u>3A4/5</u>	<u>4A11</u>	<u>2B6</u>	<u>2C8</u>	<u>2C9</u>	<u>2C19</u>	<u>2D6</u>	<u>2E1</u>
M1	0.1367	0.0719	0.2427	0.808	0.2513	0.2782	0.2092	0.0157	0.4685	0.1193	0.1132
M2	0.1285	0.0412	0.2868	0.8232	0.1628	0.3102	0.1733	0.0116	0.5409	0.1159	0.1037
M3	0.1284	0.0375	0.2944	0.8224	0.139	0.3224	0.1632	0.0091	0.5525	0.1144	0.099
M4	0.1092	0.0343	0.3222	0.7973	0.137	0.3135	0.1523	0.0088	0.5531	0.1114	0.0989

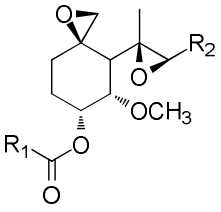
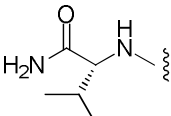
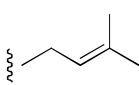
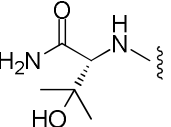
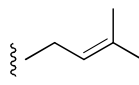
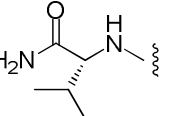
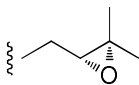
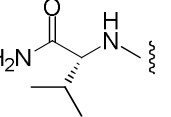
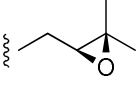
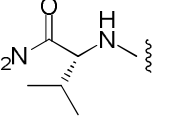
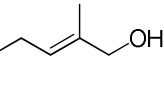
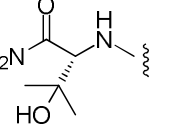
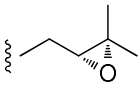
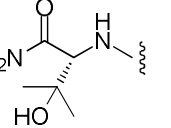
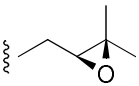
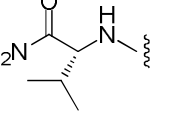
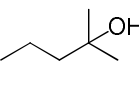
Table 2. Kinetic parameters for PPI-2458 single oxidation metabolite formation by rCYP3A4 and rCYP3A5. Results are expressed as estimate (\pm standard error).

<u>Metabolite</u>	<u>P450</u>	<u>K_m (μM)</u>	<u>V_{max}</u> ($\text{pmol min}^{-1} \text{pmol}_{\text{P450}}^{-1}$)	<u>V_{max} / K_m</u> ($\mu\text{L min}^{-1} \text{pmol}_{\text{P450}}^{-1}$)
M1	3A4	27 (2)	0.51 (0.02)	0.019 (0.002)
	3A5	17 (3)	1.58 (0.08)	0.09 (0.02)
M2	3A4	17 (2)	2.70 (0.07)	0.16 (0.02)
	3A5	17 (4)	2.86 (0.20)	0.17 (0.04)
M3	3A4	15 (2)	2.97 (0.10)	0.19 (0.02)
	3A5	17 (4)	1.42 (0.11)	0.09 (0.02)
M4	3A4	15 (3)	1.41 (0.08)	0.09 (0.02)
	3A5	26 (7)	0.80 (0.08)	0.031 (0.009)

Table 3. Kinetics of inhibition of microsomal metabolism of representative drugs. Results are expressed as estimate (\pm standard error)

<u>CYP3A Substrate</u>	<u>Modifier</u>	<u>K_i (μM)</u>	<u>K_m (μM)</u>	<u>V_{max} ($\text{nmol min}^{-1} \text{mg}_{\text{HLM}}^{-1}$)</u>
Midazolam	KTZ	0.007 (0.002)	1.7 (0.6)	2.6 (0.3)
	PPI-2458	58 (7)	1.9 (0.3)	2.6 (0.1)
Nifedipine	KTZ	0.011 (0.001)	74 (11)	2.1 (0.2)
	PPI-2458	403 (101)	87 (20)	2.2 (0.3)
Testosterone	KTZ	0.049 (0.007)	145 (48)	5.8 (1.4)
	PPI-2458	287 (48)	131 (25)	5.4 (0.8)

Table 4. Inhibition of hMetAP2 and HUVEC proliferation by metabolites and PPI-4338.

Compound			MetAP2 (% activity) ^a	HUVEC EC ₅₀ (nM)
	R1	R2		
PPI-2458			2.8	0.095
M1			1	0.3
M2			10	1.3
M3			58	6.5
M4			9	7.1
M5			6	8.8
M6			39	11.7
PPI-4338			90	ND

^aQuantitated as % activity remaining after 8 h exposure to compound.

Table 5.

A: Plasma levels of PPI-2458 and metabolites after 3 mg / kg oral dose of PPI-2458. Data given for individual animals^a

PPI-2458 ng/mL		M1 ng/mL		M2 ng/mL		M3 ng/mL		M4 ng/mL	
4 h	24 h	4 h	24 h	4 h	24 h	4 h	24 h	4 h	24 h
0.25	BLQ	BLQ	BLQ	1.7	BLQ	0.6	BLQ	1.1	0.28
0.59	BLQ	BLQ	BLQ	3.8	BLQ	1.4	BLQ	1.0	BLQ
0.82	BLQ	BLQ	BLQ	2.5	BLQ	0.94	BLQ	1.3	0.13

B: Plasma levels after 3 mg / kg oral dose of respective metabolite. Data given for individual animals^a

M1 ng/mL		M2 ng/mL		M3 ng/mL		M4 ng/mL	
4 h	24 h	4 h	24 h	4 h	24 h	4 h	24 h
1.6	0.26	0.33	BLQ	0.62	BLQ	0.82	BLQ
1.6	0.44	2.94	BLQ	0.90	BLQ	0.80	BLQ
2.3	0.10	0.54	BLQ	0.52	BLQ	0.92	BLQ

^aLimits of quantitation: PPI-2458, 0.1 ng/ml; M1, 0.1 ng/ml; M2, 0.5 ng/mL; M3, 0.1 ng/mL; M4, 0.1 ng/mL

Table 6. Free MetAP2 levels in patients treated with 15 mg doses of PPI-2458

Patient Number	Day	WBC Count ^a (x10 ³ /μL)	PD Time Point	Total Protein (mg/mL)	Free MetAP2 (ng/mL)	Percentage of Predose Free MetAP2
01-01	1	6.8	Predose	1.82	61.8	100%
			4 h	1.60	BQL ^b	<1.5%
	2	7.6	24 h	1.48	0.985	1.6%
	3	ND	48 h (prior to 2 nd dose)	1.37	4.06	6.6%
	15	7.3	Prior to Day 15 dose	1.20	6.48	10.5%
			4 h after Day 15 dose	2.47	BQL ^b	<1.5%
01-02	1	3.9	Predose	0.861	15.6	100%
			4 h	1.03	BQL ^b	<6.0%
	2	3.1	24 h	0.481	BQL ^b	<6.0%
	3	ND	48 h (prior to 2 nd dose)	0.786	2.66	17.1%

^aClinical hematology panel results from samples independent of those drawn for PD analysis

^bBQL determined to be <0.940 ng/mL from LLOQ multiplied by the lowest sample dilution factor used in the assay (0.188 ng/mL x 5)

Table 7. Pharmacokinetic parameters for PPI-2458 and its metabolites (individual and aggregated) in two NHL patients

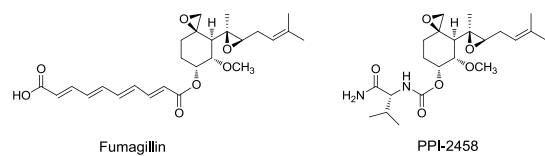
Parameter	Subject	PPI-2458	M1	M2	M3	M4	M5	M6	Summed Analytes
T _{max} (hr)	01-01	0.5	0.5	0.5	0.5	0.5	0.5	0.5	0.5
	01-02	0.7	0.7	0.7	0.7	0.7	1.1	1.1	0.7
	Average	0.6	0.6	0.6	0.6	0.6	0.8	0.8	0.6
C _{max} (ng/mL)	01-01	77.7	1.7	60.1	41.5	14.2	3.2	1.7	200
	01-02	32.3	1.6	26.6	26.1	7.2	4.9	5.0	100
	Average	55.0	1.7	43.4	33.8	10.7	4.1	3.4	150
AUC{0-t} (ng*hr/mL)	01-01	52.3	14.2	170.0	91.5	59.6	54.3	43.7	486
	01-02	35.5	3.3	69.4	68.8	18.9	22.7	23.9	242
	Average	43.9	8.8	119.7	80.2	39.3	38.5	33.8	364
AUC{0-inf} (ng*hr/mL)	01-01	52.6	NA	171.1	92.3	60.6	56.3	45.1	496
	01-02	35.6	NA	75.2	74.2	23.4	32.4	32.9	307
	Average	44.1		123.2	83.3	42.0	44.4	39.0	402
t _{1/2} (hr) ^a	01-01	2.1	NA	1.2	0.7	1.0	2.1	1.3	1.7
	01-02	1.1	NA	1.3	1.2	1.2	2.2	2.2	2.9
	Average	1.6		1.3	1.0	1.1	2.2	1.8	2.3
CL/F ^b (L/hr)	01-01	285	NA	NA	NA	NA	NA	NA	30.2
	01-02	421	NA	NA	NA	NA	NA	NA	48.9
	Average	353							39.6
V _{ss} /F ^b (L)	01-01	242	NA	NA	NA	NA	NA	NA	428
	01-02	588	NA	NA	NA	NA	NA	NA	381
	Average	415							405

^aFor metabolites, an apparent half-life reflecting the rate of elimination during the first phase, where plasma concentrations go from peak levels to levels near the lower limit of quantitation, is displayed.

^bCL/F (initial dose bioavailability adjusted clearance) and V_{ss}/F (steady-state volume of distribution) are based on the dose amount administered and are therefore computed only for PPI-2458 and the summed analytes.

Figure 1

A



B

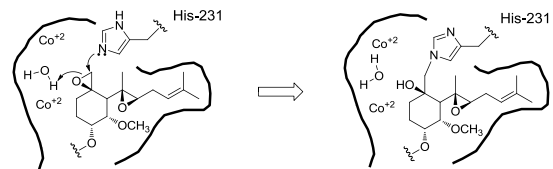


Figure 2

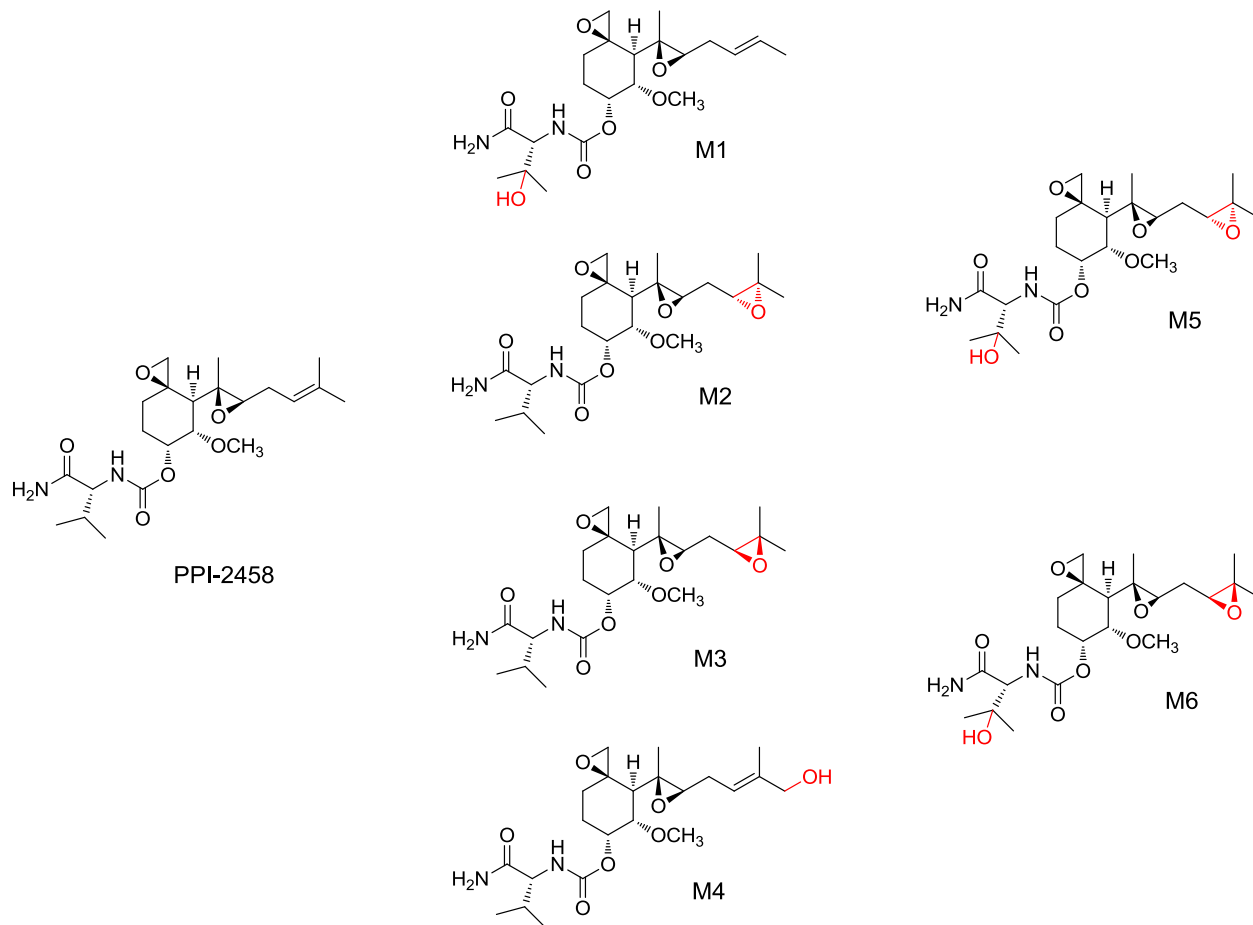


Figure 3

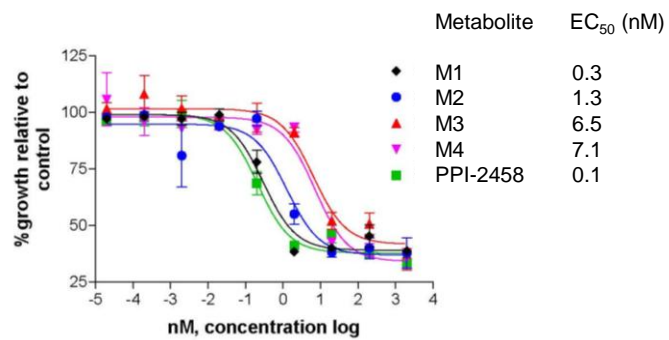


Figure 4

